Optical properties of copper clusters embedded in alumina: An experimental and theoretical study of size dependence

G. Celep, E. Cottancin,* J. Lermé, M. Pellarin, L. Arnaud, J. R. Huntzinger, J. L. Vialle, and M. Broyer
Laboratoire de Spectrométrie Ionique et Moléculaire, Université Claude Bernard Lyon I, UMR CNRS 5579, Bât. A. Kastler, 43 Bd. du 11 Novembre 1918, 69622 Villeurbanne Cedex, France

B. Palpant
Laboratoire d'Optique des Solides, Université P. et M. Curie, -Paris 6, UMR CNRS 7601, Case 80, 140 Rue de Lourmel, 75015 Paris, France

O. Boisron and P. Mélinon
Laboratoire de Physique de la Matière Condensée et Nanostructures, Université Claude Bernard Lyon I, UMR CNRS 5586, Bât. L. Brillouin, 43 Bd. du 11 Novembre 1918, 69622 Villeurbanne Cedex, France
(Received 22 March 2004; published 14 October 2004)

Optical properties of copper clusters of 3 to 5 nm in diameter, produced by laser vaporization and embedded in alumina, are investigated and compared to a semi-quantal model [based on time-dependent local-density approximation (TDLDA) and density functional theory (DFT)], including the absorption and screening properties of the ionic core background and the surrounding matrix. To begin with, the experiments show that the alumina trapped clusters are oxidized if codeposited at room temperature whereas they do remain metallic by holding the substrate temperature at 400 °C. On the other hand, reducing under H_2-N_2 atmosphere of samples made at room temperature is an alternative to elaborate embedded metallic copper clusters. Consequently, the alumina matrix evaporated on a substrate at 400 °C is optically characterized and the oxidization level of the copper clusters is carefully investigated through x-ray photoelectron spectroscopy (XPS). Concerning the optical properties of the copper clusters, a strong damping and a broadening of the surface plasmon resonance (SPR) with decreasing size is observed, in good agreement with theoretical calculations. This damping, much more important than in gold clusters, is correlated to a strong coupling of the collective excitation with interband transitions. These results allow us to validate the semiquantal model for the three systems Au, Ag, and Cu, in which the size effects are ruled by the electronic spillout phenomenon, the surface of ineffective ionic core polarization and the local porosity at the metal/matrix interface. Lastly, the inhomogeneous effects such as size dispersion are shown to be of less importance compared to intrinsic size effects in the optical properties.

DOI: 10.1103/PhysRevB.70.165409 PACS number(s): 78.67.−n, 73.22.−f, 61.46.+w, 71.15.Mb

I. INTRODUCTION

The optical response of simple metal clusters is dominated by an absorption band in the UV-visible range, the so-called surface plasmon resonance (SPR) due to the collective motion of valence *s* electrons and emerges in alkali for size as small as eight atoms per cluster.[1] Its position and width are ruled by the intrinsic properties of the clusters and the surrounding medium and appear to be size dependent. Actually, these size effects have a quantum origin and reflect the electronic structure of the clusters. For instance, the redshift of the resonance in alkali clusters when the size decreases is governed by the electron spillout phenomenon.[2] For noble metals, the *d*-core electron polarization also plays an important role.[3–6] For gold clusters embedded in alumina, the blueshift of the resonance with decreasing size is mainly due to an inner skin of ineffective screening by the *d* electrons, whose influence is predominant as compared to the spillout one.[7] In silver clusters embedded in alumina, both effects (spillout and skin of ineffective screening) are close to be compensated, inducing a quenching of size effects.[8] The good understanding of the optical properties of gold and silver clusters embedded in alumina through a mixed semiquantal model makes the extension of the study to copper clusters very attractive. In fact, it would permit to extend the validity of the model to the three systems Au, Ag and Cu belonging to the same column of the periodic table.

Little research has been done on the optical properties of copper particles. Jarrold *et al.* have investigated the absorption spectrum for very small sizes, but no clear resonance emerges and the spectrum is more complicated than the alkali ones.[9] With regard to works dedicated to larger sizes, one can see that several of them aim to develop techniques to elaborate copper cluster nanocomposite materials. It is worthy to note that the sol-gel technique needs to anneal copper oxide particles under reducing atmosphere.[10–16] Most of these studies focus on the evolution of the optical properties with the annealing temperature. Generally, copper is reduced above 200 °C under reducing atmosphere and the metallic volumic fraction increases with increasing heating temperature. Unfortunately, these methods do not allow to control and to vary the mean cluster size in the samples.

The experimental works of Manzanares-Martinez *et al.*[14] on the reduction treatments under CO atmosphere in

$Cu:SiO_2$ show that an annealing at 300 °C induces reoxidization of the particles after exposure to air whereas the reduction at 500 °C stabilizes the composition of the colloidal copper clusters. The authors think that treatments at this temperature close the porous structure of the SiO_2 films. However, Akai *et al.*[17] who elaborate nanocomposite $Cu:SiO_2$ films by sputtering and annealing under H_2 atmosphere show that the SPR disappears if the annealing temperature is too high, the copper particles being maybe reoxidized. On the other hand, the works of Serna *et al.*[18,19] show that the formation of metallic copper or oxide copper particles by pulsed laser deposition (PLD) strongly depends on the residual oxygen pressure during the deposition.

In all these works, the optical response is rather used as a signature of the metallic character of the copper particles that is revealed in photoabsorption spectra by the emergence of the SPR. To our knowledge, the only works where the cluster size and shape are controlled are those of Lisiecki *et al.* who synthesize copper metallic clusters in reverse micelles.[20–23] They obtain copper clusters in solution in the size range 2–10 nm and the photoabsorption spectra disclose a damping, broadening and very small redshift of the SPR with decreasing size. The size effects are phenomenologically interpreted by a classical model including the surface-scattering induced limited mean free path contribution of the conduction electrons in the cluster volume.[2] The broadening and damping of the SPR is well reproduced, but the model induces a strong redshift of the resonance with decreasing size that is not experimentally observed.

The originality of the present paper lies in the extension to copper clusters of previous studies performed on silver and gold ones, produced by the same laser vaporization technique and embedded in the same host matrix Al_2O_3. The only difference rests in the temperature of the substrate during deposition (see Sec. II). As for gold and silver, the optical properties are interpreted within a mixed semi-quantal model through calculations based on TDLDA formalism and density functional theory (DFT).

In Sec. II, we briefly recall the manner to obtain our $(Cu_n:Al_2O_3)$ nanocomposite films and how they are characterized. Among others, x-ray photoelectron spectroscopy (XPS) analysis allows us to tell oxidized particles from metallic ones. We then provide in Sec. II C the size evolution of the photoabsorption spectra. The results are discussed in Sec. III and compared to theoretical calculations. After a brief recall of the model ingredients, a comparison between the interband dielectric function of gold and copper will show that the damping and broadening of the SPR in copper clusters crucially depends on the exact location of the collective excitation frequency Ω_M relative to the interband transition threshold. Lastly, the influence of the size dispersion to the optical response is discussed.

II. EXPERIMENTS

A. Sample elaboration and characterization

Clusters are produced by a laser vaporization source described in previous papers.[7,23] In a small chamber under continuous flow of helium (a few tens of mbar), a rod of copper is vaporized by a frequency-doubled Nd-yttrium aluminum garnet (YAG) pulsed laser (532 nm). The so-formed metallic plasma, cooled by the inert gas, combines into clusters which expand with the inert gas through a nozzle before entering the high vacuum chamber (10^{-7} mbar) by means of a skimmer. The clusters are then codeposited with the transparent alumina matrix (evaporated thanks to an electron gun) on various substrates whose kind depends on further measurements to be performed (Suprasil, carbon coated microscope grids or silicon). The continuous helium flow allows a good stability of the cluster deposition rate. Moreover, the helium pressure is a key to controlling the mean size of the free clusters, and thus, the cluster size distribution in the samples. On the other hand, the metal volumic concentration is kept below 5% to minimize the cluster coalescence. For that, cluster and matrix deposition rates are measured by two quartz balances which also allow us to set the film thickness. The typical nanocomposite samples devoted to optical studies finally consist of a 1 cm × 1 cm square suprasil substrate of 1 mm thickness coated with about 200 nm of alumina doped with copper clusters. Identical nanocomposite materials of lower thickness (15 nm) are deposited on carbon coated grids for electron microscopy.

The production of copper clusters embedded in alumina had been already tested, but without success. At room temperature, because of a rapid oxidization, this technique fails to provide samples in which the copper particles have a metallic character. We have found that holding the substrate at a constant temperature of 400 °C during the codeposition is a mean to avoid cluster oxidization, as it will be shown and discussed below. Therefore, all the samples for which the size evolution of the optical properties is investigated have been synthesized by keeping the substrate at 400 °C under high vacuum during the codeposition. To begin with, the properties of pure alumina films deposited on a substrate held at 400 °C have been investigated, with a view to precisely determining the optical indexes, the stoichiometry and the porosity of the matrix. First, ellipsometry measurements allowed us to obtain the optical indexes in the energy range 300–800 nm. The index $n(\omega)$ is slightly higher than the one obtained for alumina deposited at room temperature. Between 300 and 800 nm, $n(\omega)$ varies from 1.71 to 1.65 at 400 °C and from 1.64 to 1.60 at room temperature. The increase of the optical index n (at 400 °C) is correlated to a lower porosity. Indeed thickness measurements show that the average porosity is around 30% with respect to crystalline alumina (instead of 45% for alumina deposited at room temperature). On the other hand, Rutherford back scattering (RBS) measurements on pure alumina samples give the average stoichiometry $Al_2O_{3.2}$, the same as the one obtained for alumina deposited at room temperature. Finally, one can conclude that the alumina matrix deposited at 400 °C has an amorphous structure with a porosity of 30% compared to anodic alumina, is transparent between 1 and 5.1 eV and its averaged stoichiometry is $Al_2O_{3.2}$. The size distributions in the samples containing copper clusters are determined from transmission electron microscopy (TEM). TEM micrographs are given in Fig. 1 for three samples obtained with three different helium pressures in the source.The particles are al-

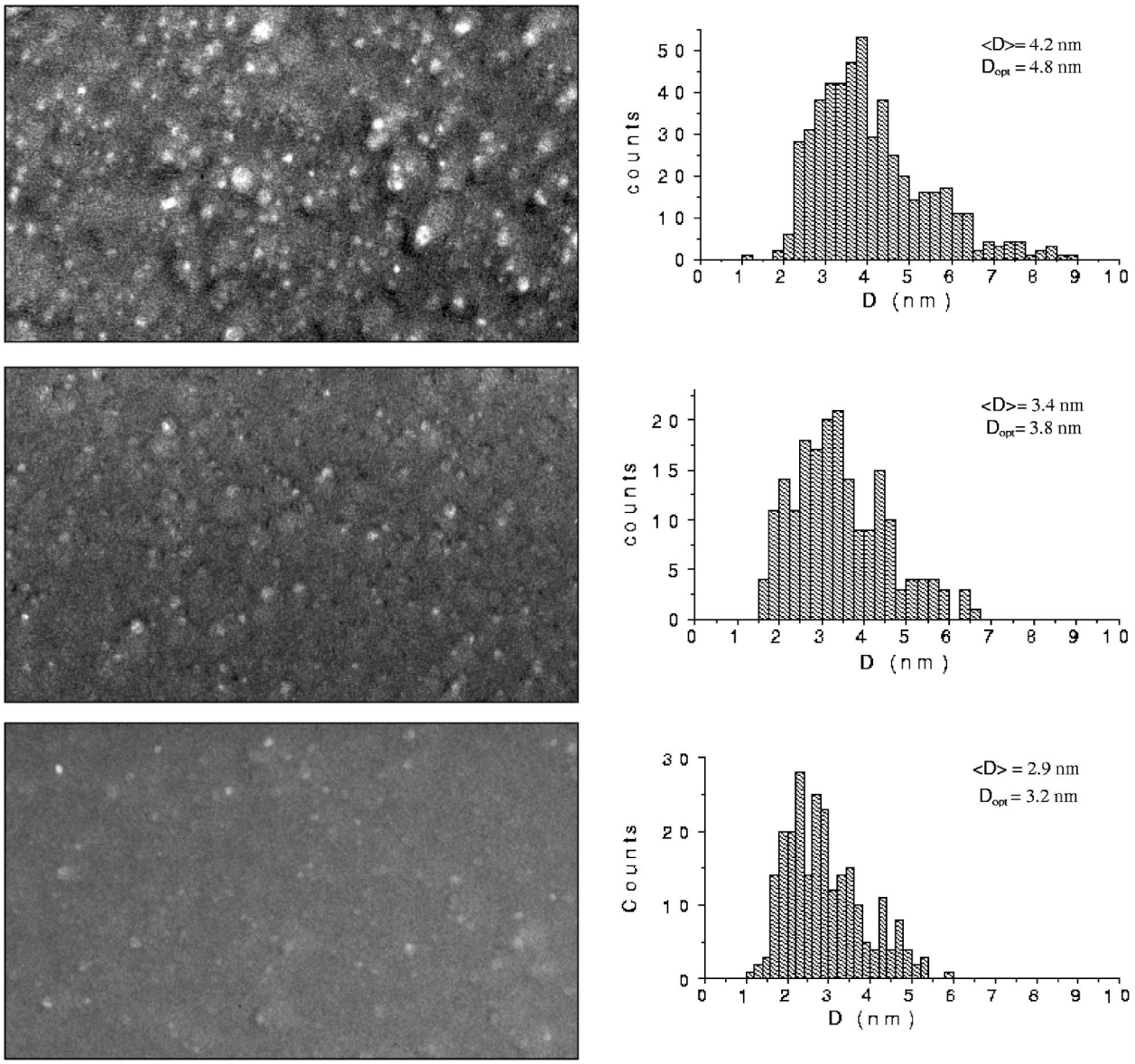

FIG. 1. Left: TEM micrographs of three samples of Cu_n clusters embedded in alumina and deposited at $T_{sub}=400$ °C. Right: Size distribution of copper clusters deduced from the TEM micrographs. $\langle D\rangle$ and D_{opt} design the mean diameter and the optical diameter, respectively.

most spherical and randomly distributed in the transparent matrix. The size distributions are deduced from micrographs over a population of around 300 particles per sample and reported on the right side of Fig. 1. Their widths [full width at half maximum (FWHM)] are around 80% of the mean cluster diameter. The optical diameter[7] $D_{opt}=\sqrt[3]{\langle D^3\rangle}$ varies from 3 to 5 nm, corresponding to a mean number of atoms per cluster between 1200 and 5500.

B. Influence of the substrate temperature and of annealing of the sample

Let us focus attention to the effects induced by the substrate temperature. As is made clear by Fig. 2(a) the optical response of the nanocomposite materials strongly depends on the temperature of the substrate during the codeposition. At room temperature the expected SPR band does not appear, suggesting that copper clusters have been completely oxidized during the codeposition. If the substrate is kept at 400 °C (as explained in Sec. II A), the optical spectra of the samples agree qualitatively with the expected theoretical response of metallic copper particles embedded in alumina (i.e., the emergence of the SPR band and the steady increase of the absorption beyond the interband transition threshold of copper). And yet, the analysis of the TEM micrographs shows that the size distributions of the clusters, produced under the same source conditions, are still the same in both cases.

A classical Mie calculation in the dipolar approximation has been performed assuming the presence of $(CuO)_n$ or $(Cu_2O)_n$ clusters in the matrix; the calculated absorption spectra, for which the dielectric functions of CuO and Cu_2O

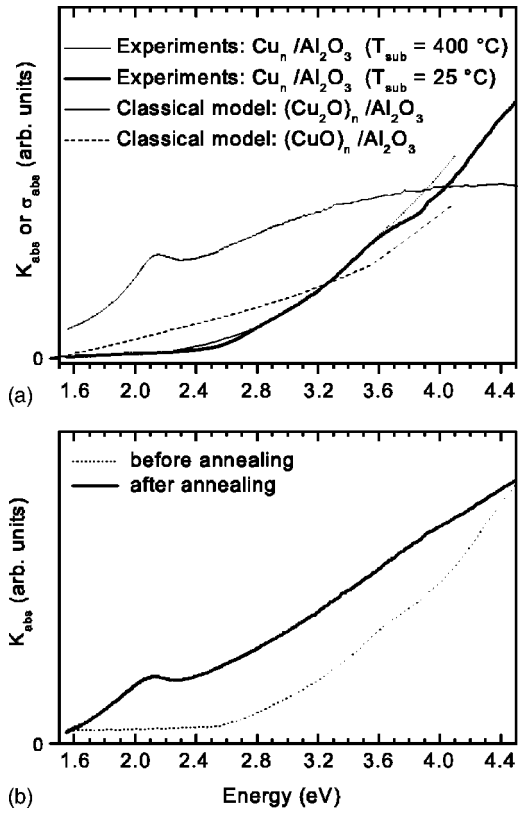

FIG. 2. (a) Experimental absorption spectra obtained for copper clusters codeposited with alumina, either at room temperature, or at 400 °C. Comparison with theoretical absorption spectra of $(CuO)_n$ or $(Cu_2O)_n$ clusters in alumina. (b) Absorption spectra of the sample before and after annealing under H_2-N_2 atmosphere at 300 °C for 25 min.

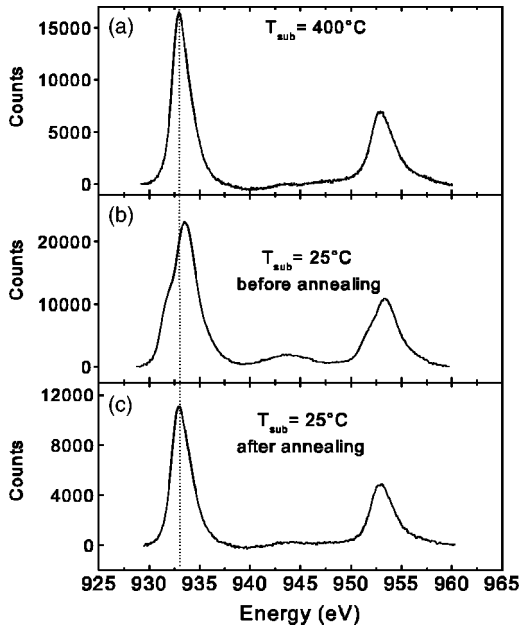

FIG. 3. XPS Cu $2p\frac{3}{2}$ and Cu $2p\frac{1}{2}$ levels of three samples of alumina embedded copper clusters. (a) Sample made with a substrate held at 400 °C. (b) Sample made with a substrate held at room temperature before annealing. (c) Same sample as (b) after annealing under $H_2(5\%)$-$N_2(95\%)$ atmosphere for 25 min. at 300 °C.

have been extracted from the tables of Ref. 24 are plotted in Fig. 2(a). The spectrum obtained for $(Cu_2O)_n$ clusters is in good agreement with the experimental one obtained for the sample made at room temperature. Moreover, the experimental response is similar to the one obtained for silica film doped with Cu_2O nanoparticles of 2 nm (increase of the absorption above 2.5 eV).[25] Consequently, one can reasonably think that the codeposition at room temperature induces oxidization of copper clusters with a stoichiometry near Cu_2O.

On the other hand, a sample was synthesized at room temperature and annealed afterwards at 400 °C under high vacuum. Even so, the absorption spectrum indicates that the copper clusters remain oxidized. So, the clusters are actually oxidized during the codeposition. Keeping in mind that alumina is overstoichiometric in oxygen, one can suppose that this excess in oxygen contributes to the oxidization of copper at room temperature. By holding the substrate at 400 °C the temperature may be high enough to prevent from the adsorption of oxygen on copper clusters and so to prevent from their oxidization.

Another possibility to take cautions against cluster oxidization is to remove oxygen after deposition by annealing under reducing atmosphere. The optical response of a sample made at room temperature before and after annealing under $H_2(5\%)$-$N_2(95\%)$ atmosphere (at $P=1$ atm for 25 min at 300 °C) is displayed in Fig. 2(b). The response after annealing is characteristic of metallic copper particles in alumina, which is a telltale sign of the reduction of the oxidized copper clusters.

Furthermore, x-ray photoelectron spectroscopy (XPS) experiments, carried out on samples obtained with a substrate, either at 400 °C, or at room temperature, before and after annealing under H_2-N_2 atmosphere, confirm the previous results. Figure 3 displays the recorded spectra for the three cases. At 400 °C, an Auger peak is detected at 918.1 eV, that can be attributed, to either Cu or CuO.[26] The Auger peak corresponding to Cu_2O does not appear. On the other hand, the XPS spectrum [see Fig. 3(a)] exhibits a peak at 932.8 eV attributed to Cu or Cu_2O (the peak corresponding to CuO is not detected. From these two results, one can easily conclude that the clusters are not oxidized. If the sample is made at room temperature, the XPS spectrum is shifted. Moreover, the resulting peak is the fruit of two underlying peaks. The position of the main one is at 933.5 eV characteristic of CuO.[25,26] The other one is at about 932.2 eV corresponding to Cu or Cu_2O. The analysis of the Auger peaks allows one to conclude that this second peak is the signature of the presence of Cu_2O. Furthermore, the occurrence of a weak satellite peak between the two main ones confirms the presence of CuO. So, it is clear from these findings that the particles obtained at room temperature are oxydized copper clusters $[(Cu_xO)_n$ with $x=1$ or $x=2]$. After annealing under $H_2(5\%)$ -$N_2(95\%)$ atmosphere, the XPS spectrum is the same as the one obtained for the sample made at 400 °C, showing that the $(Cu_xO)_n$ particles have been completely reduced during annealing.

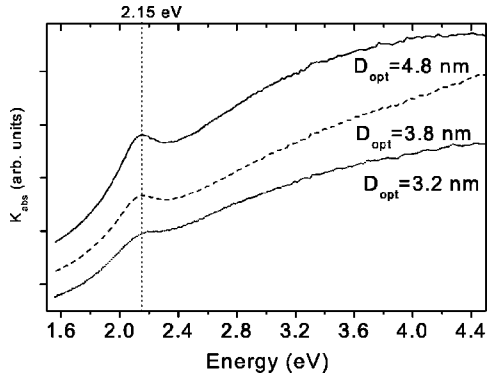

FIG. 4. Size evolution of the experimental absorption spectra of copper clusters versus energy. The three spectra correspond to the samples of Figure 1.

C. Size evolution of the optical response of copper clusters

Optical transmission measurements are performed with a Perkin-Elmer spectrophotometer in the energy range 1.55–4.51 eV (275–800 nm) under Brewster incidence, using *p*-polarized light (the electromagnetic field $\vec{E}$ being in the incidence plane). It has already been shown that this method permits us to remove oscillations in the transmission spectra due to multiple reflexion effects.[27] The size evolution of the absorption spectra is displayed in Fig. 4. The three spectra correspond to the samples performed with a substrate kept at 400 °C during the codeposition and whose size distributions are given in Fig. 1. The damping of the SPR band emerging from the increase of the interband transitions, with decreasing size is the most important feature of the experimental observations. Moreover, a broadening of the SPR with decreasing size is also patent. We will see that the damping of the resonance is a signature of a slight blueshift of the SPR frequency with decreasing size and is actually an intrinsic size effect. Nevertheless, the damping may be also, to a lower extent, connected to inhomogeneous effects (size, shape, and local porosity).

III. THEORY AND DISCUSSION

A. Calculation of the optical response of embedded copper clusters

In order to interpret the experimental absorption spectra, in particular the size evolution of the plasmon-band features which—in the studied size range—reflect to a large extent quantum finite-size effects, calculations have been carried out in the framework of a mixed semiquantal model. This model was previously applied for explaining the size dependence of the optical properties of matrix-embedded Ag_n and Au_n clusters,[8] and subsequently of alloyed $(Au_xAg_{1-x})_n$ clusters[28,29] in its improved version.[30] For pure Ag and Au metal clusters, the size evolution of the SPR frequency was found to be ruled by the competition between opposite size trends, namely the redshift and blueshift trends induced by, respectively, (i) the spillout effect and (ii) the surface layer of ineffective ionic core polarizability and the local porosity at the metal/matrix interface.

As compared to simple metals, such as alkali,[1,31,32] the optical properties of noble metal clusters are more complex because interband transitions occur in the visible-ultraviolet spectral range. These transitions correspond to electronic excitations from fully occupied *d*-valence electron bands located close below the Fermi energy E_F (3*d*, 4*d*, and 5*d* for Cu, Ag, and Au, respectively) to unoccupied levels above E_F. The interband thresholds $\hbar\Omega_{ib}$ for silver, gold, and copper are on the order of 4, 2, and 2 eV, respectively. Moreover these interband transitions (i.e., the ionic core polarization) are responsible, through dynamical screening effects, for a strong shift towards lower energies of the surface plasmon or SPR frequency ω_M and, in addition, for a strong damping and broadening of the resonance band in the case of Au_n and, as it will be seen, of Cu_n particles ($\Omega_{ib} < \omega_M$).

The calculations are based on the time-dependent local-density-approximation formalism (TDLDA) and the density functional theory (DFT), within a model including the absorption and screening properties of both the ionic core background and the surrounding matrix.[30] This model has been detailed and discussed in previous papers, so we only recalled the main ingredients here, with particular focusing on the most relevant parameters or model inputs ruling the size effects.

The conduction electrons, responsible for the collective surface plasmon excitation and underlying most of the quantum finite-size effects, are quantum mechanically treated, whereas the ionic background is phenomenologically described by both: (i) a step-walled homogeneous spherical charge distribution (jellium) of radius $R=r_sN^{1/3}$ [r_s is the Wigner-Seitz (WS) radius per conduction electron in the bulk] and (ii) a homogeneous dielectric medium [core-electron complex dielectric function $\varepsilon_{ib}(\omega)$, corresponding to the interband transitions, assumed to be bulklike] extending up to $R_c=R-d$ where *d* is the skin thickness of ineffective ion polarizability. This ingredient, introduced early by Liebsh[33] in the context of electron energy loss at metal surfaces, and discussed later by several authors,[34–36] is thought to be related to the spatial localization of the *d*-electron wave functions.[35] The value $d=3$ a.u. (1 a.u. $=0.529$ Å), slightly lower than the one involved for Ag and Au particles ($d=3.5$ a.u.[8]), has been selected for Cu_n particles, in assuming the rough scaling law $d(\mathrm{Cu}) \approx d(\mathrm{Ag,Au})[r_s(\mathrm{Cu})/r_s(\mathrm{Ag,Au})]$ (smaller ion-core size for copper). The complex dielectric function $\varepsilon_{\mathrm{ib}}(\omega)$, that is an input data of the model, has been carefully extracted from the experimental complex dielectric function $\varepsilon_{\mathrm{exp}}(\omega)$ of bulk copper[24] a Kramers-Kronig analysis after subtracting the conduction-electron contribution $\varepsilon_s(\omega)$, parametrized as a Drude-Sommerfeld formula (see Refs. 34 and 37 for the details of the procedure). For this extraction we have assumed $\hbar\Omega_{ib}=1.85$ eV [extrapolation to zero of the steep rising edge of the imaginary component of $\varepsilon_{\mathrm{exp}}(\omega)$ near 2 eV]. The contribution $\varepsilon_s(\omega)$ of the conduction electrons to the overall dielectric function $[\varepsilon_{\mathrm{exp}}(\omega)=\varepsilon_s(\omega)+\varepsilon_{ib}(\omega)-1]$ is

$$\varepsilon_s(\omega) = 1 - \frac{\omega_p^2}{\omega(\omega + i\Gamma)} \tag{1}$$

with the following parameters: plasma frequency $\omega_p = \sqrt{3/r_s^3 m}$, effective electron mass $m=1.42$ a.u.,[37] W.S. radius

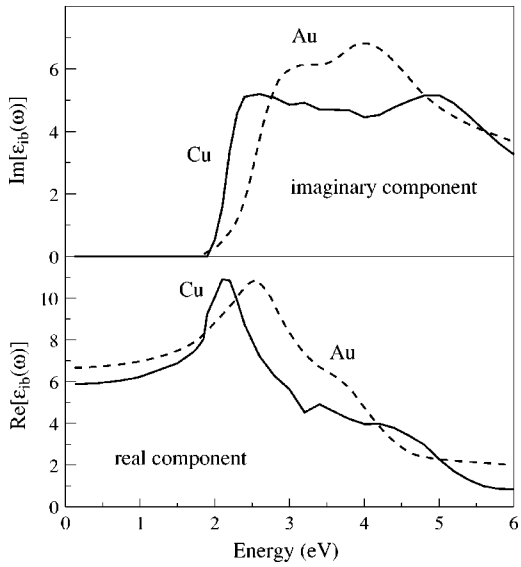

FIG. 5. Spectral dependence of the imaginary (upper figure) and real (lower figure) components of the complex dielectric functions $\varepsilon_{ib}(\omega)$ corresponding to the interband transitions, for copper (full line curves) and gold (dashed line curves).

$r_s \approx 2.67$ a.u.,[38] $\hbar\Gamma(\infty)=0.12$ eV [$\hbar\Gamma(\infty)$ has been determined from the analysis carried out in the spectral range around the interband threshold, namely, the spectral range of interest].

The imaginary and real component of $\varepsilon_{ib}(\omega)$ for copper are shown in Fig. 5, and compared with those previously determined for gold.[34] From the similarity of both interband dielectric functions the absorption properties for copper particles are expected to be qualitatively similar to those obtained for gold (for both metals ω_M is located just above Ω_{ib}). Let us emphasize, however, that the parameters r_s and m are noticeably different (for Au, $r_s \approx 3.01$ a.u. and $m \approx 1$ a.u.) and the present calculations are actually a test for assessing the suitability of the present semiquantal multilayered dielectric model.

With respect to the matrix, the dielectric function of porous alumina deposited on warmed substrates (see Sec. II A), determined by ellipsometry measurements, has been used in the calculations. Moreover, due to the local porosity at the metal/matrix interface (surface roughness, contact defects,….[8]), that results in a lowering of the local effective matrix polarizability, a vacuum rind of thickness d_m is introduced in the model in order to mimic the spherically averaged local porosity. Since the samples have been elaborated under the same experimental deposition conditions as in our previous works on Ag and Au clusters (except for the substrate heating[8]), the same value as in our previous studies ($d_m=2$ a.u.) has been selected in the present calculations.

The absorption cross sections

$$\sigma(\omega) = \frac{4\pi\omega}{c\varepsilon_m^{1/2}} \mathrm{Im}[\alpha(\omega)] \tag{2}$$

[$\alpha(\omega)$ is the dynamical polarizability] calculated for various cluster sizes[39] are shown in Fig. 6. Since the magnitude of the cross-section scales roughly as the particle volume the theoretical data have been multiplied by the factor $15\,000/N$ (the y axis corresponds thus strictly to the largest size $N=15\,000$). This scaling allows to plot all the spectra in the same figure and makes the size evolution of the resonance band more apparent.

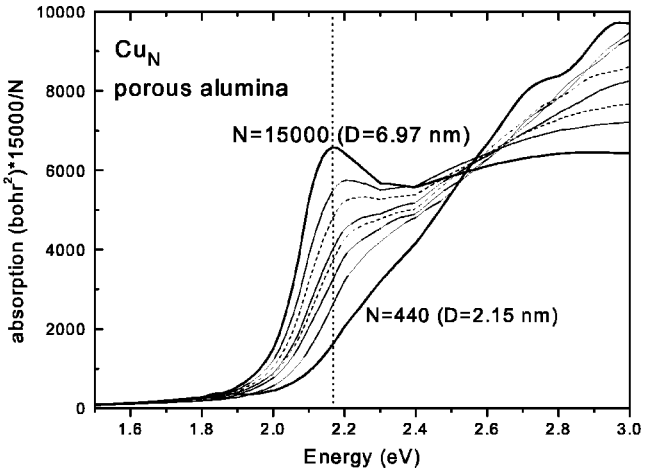

FIG. 6. Absorption cross sections calculated within the semiquantal model (TDLDA formalism), for various alumina-embedded Cu_n cluster sizes $N=440$ (diameter $D=2.15$ nm), 832 (2.7 nm), 1314 (3.1 nm), 2048 (3.6 nm), 3438 (4.3 nm), 5670 (5 nm), 8000 (5.65 nm), and 15 000 (6.97 nm). The theoretical data have been multiplied by the volumic ratio $15\,000/N$. The model involves a surface layer of ineffective ionic-core polarization (thickness $d=3$ a.u.) and a vacuum rind of thickness $d_m=2$ a.u. at the metal/matrix interface simulating the local porosity. The figure displays the results obtained when the measured dielectric function of porous alumina deposited on a warmed substrate is used ($\varepsilon_m \approx 2.75$ around 2.2 eV).

This figure shows that the resonance band (around 2.17 eV) emerges gradually from the rising edge of the interband transitions as the particle size increases, as for gold clusters (for gold the resonance band, located around 2.25 eV, is, however, much more apparent[7,34]). Qualitatively, and also quantitatively (if one excepts the slight blueshift which is not obvious in experiment), the calculations are in very good agreement with the experiment. As a matter of fact, a strict comparison with the experimental spectra would require to take into account the size, shape and local environment (interface) distributions for each sample. All these distributions would result in a smoothing of the absorption cross section by inhomogeneous effects. A more reliable test of the theoretical predictions would require samples involving much less broad distributions. Work is in progress in our laboratory in order to obtain a much better size selection and to extend the range of the available cluster sizes (very small or very large).

On the other hand, the size effects we experimentally observe can not be phenomenologically described by a classical model including the surface-scattering induced limited mean free path contribution of the conduction electrons in the cluster volume.[2] Indeed, this model predicts a redshift of the SPR with decreasing size without major damping and broadening, in total opposition with the observed broadening and damping of the SPR.

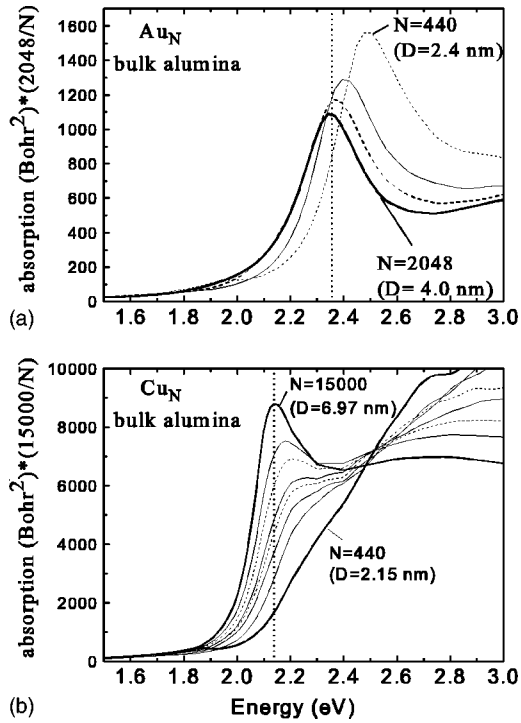

FIG. 7. Absorption cross sections calculated within the semiquantal model (TDLDA formalism). (a) For bulk alumina-embedded Au_n cluster sizes $N=440$ (diameter $D=2.4$ nm), 832 (3.0 nm), 1314 (3.5 nm), 2048 (4.1 nm) ($d=3.5$ a.u., $d_m=2$ a.u.). (b) For bulk alumina-embedded Cu_n cluster sizes corresponding to Fig. 6 ($d=3.0$ a.u., $d_m=2$ a.u.). The figures show the results obtained when the dielectric function of bulk alumina is involved in the model calculations ($\varepsilon_m \approx 3.13$ around 2.2 eV).

B. On the emergence of the surface plasmon resonance

From Fig. 5 it is also suggested that, due to the much steeper increase of $\mathrm{Im}[\varepsilon_{ib}(\omega)]$ above the interband threshold $\hbar\Omega_{ib}$ (as compared to gold), the damping and broadening of the surface plasmon band in Cu_n clusters will depend more strikingly on the exact location of the collective excitation frequency ω_M relative to $\hbar\Omega_{ib}$: significant qualitative modification of the absorption spectrum around 2 eV may result from very small change of the SPR frequency. From an experimental point of view, this remark points out that well-controlled elaboration conditions and a careful sample characterization are necessary for interpreting with reliability the optical properties of composite samples involving copper particles. Correspondingly, from a theoretical point of view, the plasmon band shape will be very sensitive to the input parameters of the model, in particular the dielectric function of the surrounding matrix.

To illustrate the difference between gold and copper clusters, the optical responses of gold clusters and copper clusters embedded in bulk-alumina are given in Fig. 7. The comparison with copper emphasizes that the emergence of the SPR is very sensitive to the slope of the rising edge of $\mathrm{Im}[\varepsilon_{ib}(\omega)]$ above the interband threshold. Indeed, the SPR is clearly visible for small sizes in the case of gold whereas the plasmon band is only reflected through a shoulder superimposed on the rising edge of the interband transitions above $\hbar\Omega_{ib}$ in the case of copper. Moreover, for copper clusters, as stressed above, the absorption spectrum, in particular the emergence of the resonance band and its shape, strongly depends on the dielectric function of the surrounding matrix that rules to a large extent the location of the SPR frequency relative the interband threshold (see Figs. 6 and 7). The steady size evolution of the damping and broadening of the resonance band is actually a direct signature of the slight blueshift trend of the resonance frequency ω_M as the size decreases.

The correlation between the blueshift of the resonance frequency ω_M and the damping and broadening of the SPR can be explained in the picture of "a discrete state coupled with a continuum."[40] The energy of the electronic state corresponding the collective excitation ("surface plasmon state") lying in the quasicontinuum associated with the interband excitations (one-electron *d-sp* excitations), the oscillator strength corresponding to the transition between the ground state and the surface plasmon state is therefore spread over a large spectral range. As the size decreases the resonance frequency ω_M is slightly blueshifted (as for gold particles the blueshift trend overcomes the spillout-induced redshift trend[7,8,34]) and the broadening of the band—and consequently the damping—becomes larger. This is because the joined density of states around $E=\hbar\omega_M$ increases as the energy increases: as the energy increases above the interband threshold $E_{ib}=h\Omega_{ib}$ more and more occupied *d* states and unoccupied conduction states contribute to the interband excitations in a given spectral range ΔE. The strong increase of the joined density of states (*d-sp* transitions) is actually the main factor underlying the very steep rising edge of $\mathrm{Im}[\varepsilon_{ib}(\omega)]$ above $\hbar\Omega_{ib}$. Let us remark that part of the Landau damping stems also from the coupling with the one-electron conduction-electron intraband excitations.

The sensitivity of the absorption cross section to various input model parameters has been carefully investigated. First, the results do not depend very strongly on the thickness of the surface skin of ineffective polarizability. The value $d=3.5$ a.u. used for gold and silver clusters,[8] determined by comparison with experimental data on free Ag_n^+ clusters, yields an almost imperceptible change of the Mie's peak pattern. On the other hand, the emergence of the resonance band and its exact location depends noticeably on the refractive index of the surrounding matrix (see Fig. 6). On Fig. 8 are compared the results of the present mixed semiquantal model and those obtained within the classical theory in the dipolar approximation (quasistatic), for the largest studied size $N=15\,000$ ($D\approx 7$ nm). The standard Mie's calculation [a single dielectric interface[41] ($d=d_m=0$) and the "quantum" absorption spectrum ($d=3$ a.u., $d_m=2$ a.u.; thick full line curve) are quite similar, pointing out that—in this size range—the blueshift and redshift trends induced by the surface effects balance almost perfectly. Let us recall that no size dependence in the absorption cross section is predicted within the standard Mie's theory (for $\lambda \ll D$), except for a mere volume scaling factor. In many theoretical investigations a size-dependence is phenomenologically introduced by taking into account the so-called surface scattering-limited mean-free-path effect[2,42] through a *R*-dependent electron scattering rate of the form $\Gamma(R)=\Gamma(\infty)+Av_F/R$ (v_F is

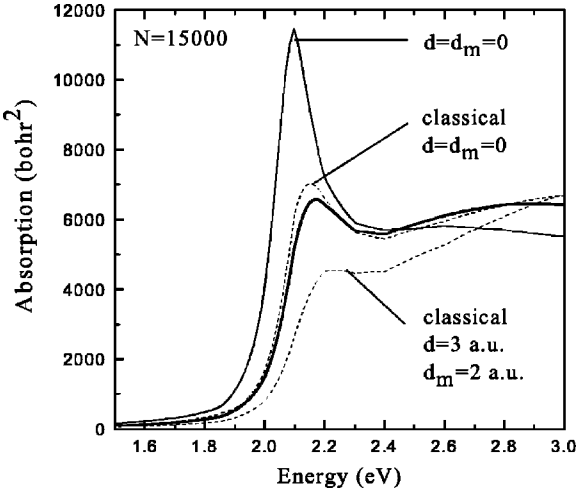

FIG. 8. Sensitivity of the absorption cross-section to the input parameters. Only the modified parameters, relative to the "standard" model calculations ($d=3$ a.u., $d_m=2$ a.u., dielectric function of porous alumina) reported in Fig. 6 are indicated. Comparison between the quantum results (full line curves) and the classical predictions (dashed line curves).

the Fermi velocity and A a model-dependent parameter) in the Drude parametrization of the dielectric function associated to the conduction electron excitations. The surface contribution in the electron scattering time is indeed strongly dependent on the metal, the matrix and the interface (defects, chemical bonding, etc.[42]), and the parameter A is in general considered as a free model parameter. Although this ingredient is able to ensure the broadening and damping of the Mie resonance observed in small particles, it yields however a spurious large redshift of the resonance for small sizes **(**see, for instance, Refs. 20 and 22 in the case of copper clusters [Fig. 1 and 1(a), respectively], or Ref. 6 in the case of gold clusters (Fig. 8)**)**, and is thus unable to reproduce the experimental findings. In including the surface skins of vanishing polarizability in the classical calculations ($d=3$ a.u. and $d_m=2$ a.u., three dielectric interfaces, thick dashed line curve), a size dependence for the Mie's frequency ω_M is obtained (blueshift trend as the size decreases) but the plasmon band is much more blueshifted—and consequently damped—compared to the quantum results. Such a difference stems obviously from the electron spillout effect which is not taken into account in the classical approach. The importance of this quantum effect in the case of copper is clearly evidenced in Fig. 8. This is due to the low r_s value in copper and the strong correlation between the location of the Mie's frequency and the damping of the plasmon band arising. This last feature is the main factor responsible for the very slow convergence of the calculated absorption spectrum towards the standard Mie's spectrum ($d=d_m=0$) as the size increases.

C. Influence of the size dispersion on the optical response of copper embedded clusters

Finally, the influence of the size distribution of the sample in the optical response has been investigated through classical calculations. In Fig. 9 are displayed the calculated absorption spectra, in taking into account the size distributions shown in Fig. 1, for various model parameter values. Figure 9(a) shows the results obtained with $d=d_m=2$ a.u. The value $d=2$ a.u., lower than the one involved in the semiquantal model, is an *ad hoc* parameter chosen in order to roughly compensate the fact that the spillout effect is disregarded in a classical approach (a skin of lower thickness reduces the induced-blueshift trend). In Fig. 9(b) only the local porosity is taken into account ($d=0$ and $d_m=2$ a.u.) whereas no size effects are included in the results displayed in Fig. 9(c) ($d=0$ and $d_m=0$). In this last case all the spectra are the same except for a mere scaling factor and the SPR appears clearly. Indeed the frequency location of the SPR is redshifted and the coupling between intraband and interband transitions less important. When the local porosity is involved in the model [Fig. 9(b)], the damping of the SPR is clearly patent. This is due to the small blueshift of the resonance peak which increases the coupling of the collective excitation with interband transitions. When the skin of reduced polarizability is included in the model, the blueshift is larger and thus, the damping is still more important [Fig. 9(a)]. The size evolution of the absorption spectra (damping and broadening) in

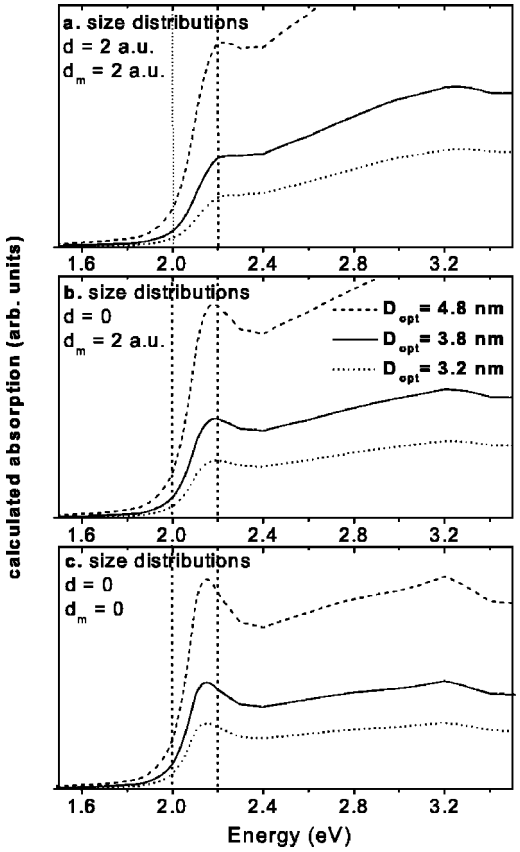

FIG. 9. Classical simulations of the experimental absorption spectra by taking into account the size distributions displayed in Fig. 1. (a) Calculations with a local porosity ($d_m=2$ a.u.) and a skin of reduced polarizability ($d=2$ a.u.). (b) calculations with a local porosity ($d_m=2$ a.u.) and with $d=2$ a.u.. (c) calculations without size and surface effects ($d=0$ and $d_m=0$). The calculations are performed for copper clusters embedded in porous alumina (dielectric function of porous alumina deposited on a warmed substrate).

this case is in good qualitative agreement with the experimental ones and with the results obtained for a single size in the semiquantal model. These calculations underlie the importance of the intrinsic surface effects, namely, the skin of reduced ion polarizability and the local porosity, which, in the case of copper, overcome those resulting from inhomogeneous effects. Even if the size dispersion induces a slight damping and broadening, the main size effects experimentally observed remain correlated to intrinsic ones. This small influence of the size distribution is explained by the fact that the optical response is mainly due to the tail of the distribution, the response being proportional to the volume of the particles.

IV. CONCLUSION

In this paper, nanocomposite samples of alumina doped with metallic copper clusters of various mean size have been elaborated by an original physical way. The influence of the substrate temperature to the oxidization of the copper particles has been investigated. We have checked that the metallic character of copper clusters is preserved when the samples are synthesized at high temperature (400 °C). Moreover, annealing under H_2-N_2 atmosphere has been proved to be an alternative to produce metallic copper clusters.

The size evolution of their optical properties has been investigated in the size range 3–5 nm in diameter. The damping and broadening with decreasing size of the surface plasmon resonance (SPR) band are in good agreement with the semiquantal model, based on TDLDA formalism and DFT, already used for silver and gold clusters. The comparison with the results obtained for gold shows that, in spite of quite similar interband dielectric functions in gold and copper, the damping of the SPR band with decreasing size is much more dramatic in copper, so as the resonance completely vanishes below 2 nm in diameter, while it persists in gold clusters. This vanishing of the SPR cannot be explained by classical theories, only the semiquantal model permits one to interpret these experimental results. Consequently this semiquantal model is demonstrated to be suitable to interpret the optical properties of all noble metal clusters (Au, Ag, and Cu) in the size range 2–10 nm.

ACKNOWLEDGMENTS

The authors are grateful to P. Thévenard and J.L. Rousset for fruitful discussion. Many thanks to A. Bourgey, C. Clavier, G. Guiraud, and F. Valadier, for their essential technical support. Thanks to C. Journet and S. Purcell who gave us access to their annealing furnace.

*Electronic address: cottanci@lasim.univ-lyon1.fr

[1] W. A. D. Heer, Rev. Mod. Phys. **65**, 611 (1993).
[2] U. Kreibig and M. Vollmer, *Optical Properties of Metal Clusters* (Springer, Berlin, 1995).
[3] J. Tiggesbäumker, L. Köller, H. Lutz, and K. Meiwes-Broer, Chem. Phys. Lett. **190**, 42 (1992).
[4] J. Tiggesbäumker, L. Köller, K. H. Meiwes-Broer, and A. Liebsch, Phys. Rev. A **48**, R1749 (1993).
[5] S. Fedrigo, W. Harbich, and J. Buttet, Phys. Rev. B **47**, 10 706 (1993).
[6] M. Alvarez, J. Khoury, T. Schaaff, M. Shafigullin, I. Vezmar, and R. Whetten, J. Phys. Chem. B **101**, 3706 (1997).
[7] B. Palpant, B. Prével, J. Lermé, E. Cottancin, M. Pellarin, M. Treilleux, A. Pérez, J. L. Vialle, and M. Broyer, Phys. Rev. B **53**, 1963 (1998).
[8] J. Lermé, B. Palpant, B. Prével, M. Pellarin, M. Treilleux, A. Pérez, J. L. Vialle, and M. Broyer, Phys. Rev. Lett. **80**, 5105 (1998).
[9] M. Jarrold and K. Creegan, Chem. Phys. Lett. **166**, 116 (1990).
[10] M. Nogami, Y. Abe, and A. Nakamura, J. Mater. Res. **10**, 2648 (1995).
[11] D. Kundu, I. Honna, T. Osawa, and H. Komiyama, J. Am. Ceram. Soc. **77**, 1110 (1994).
[12] G. De, M. Epifani, and A. Licciulli, **201**, 250 (1996).
[13] G. De, M. Gusso, L. Tapfer, M. Catalano, F. Gonella, G. Mattei, and G. Battaglin, J. Appl. Phys. **80**, 6734 (1996).
[14] J. Manzanares-Martinez, L. A. Garcia-Cerda, R. Ramirez-Bon, F. J. Espinoza-Beltran, J. F. Perez-Robles, and J. Gonzalez-Hernandez, Thin Solid Films **365**, 30 (2000).
[15] J. F. Pérez-Nobles, F. J. Garcia-Rodriguez, J. M. Yanes-Limon, F. J. Espinoza-Beltran, Y. V. Vorobiev, and J. Gonzalez-Hernandez, J. Phys. Chem. Solids **60**, 1729 (1999).
[16] T. Lutz, C. Estournès, J. Merle, and J. Guille, J. Alloys Compd. **262–263**, 438 (1997).
[17] T. Akai, K. Kadono, H. Yamanaka, T. Sakagushi, M. Miya, and H. Wakabayashi, J. Ceram. Soc. Jpn. **101**, 105 (1993).
[18] R. Serna, D. Babonneau, A. Suarez-Garcia, and C. N. Afonso, Phys. Rev. B **66**, 205402 (2002).
[19] J. Gonzalo, R. Serna, J. M. Requejo, J. Solis, C. N. Afonso, and A. Naudon, Appl. Surf. Sci. **154–155**, 449 (2000).
[20] I. Lisiecki and M. Piléni, J. Am. Chem. Soc. **115**, 3887 (1993).
[21] I. Lisiecki and M. Piléni, J. Phys. Chem. **99**, 5077 (1995).
[22] I. Lisiecki, F. Billoudet, and M. P. Pileni, J. Phys. Chem. **100**, 4160 (1996).
[23] M. Pellarin, B. Baguenard, M. Broyer, J. Lermé, J. L. Vialle, and A. Perez, J. Chem. Phys. **98**, 944 (1993).
[24] E. D. Palik, *Handbook of Optical Constants of Solids* (Academic Press, New York, 1985/1991), Vols. I and II.
[25] K. Borgohain, N. Murase, and S. Mahamuni, J. Appl. Phys. **92**, 1292 (2002).
[26] J. Moulder, W. Stickle, P. Sobol, and K. Bomben, *Handbook of X-ray Photoelectron Spectroscopy* (Perkin-Elmer, Eden Prairie, 1992).
[27] M. Gaudry, E. Cottancin, M. Pellarin, J. Lermé, J. Huntzinger, J. Vialle, M. Broyer, J. Rousset, M. Treilleux, and P. Mélinon, Phys. Rev. B **67**, 155409 (2003).
[28] E. Cottancin, J. Lermé, M. Gaudry, M. Pellarin, J. L. Vialle, M. Broyer, B. Prével, M. Treilleux, and P. Mélinon, Phys. Rev. B **62**, 5179 (2000).
[29] M. Gaudry, J. Lermé, E. Cottancin, M. Pellarin, B. Prével, M.

Treilleux, P. Mélinon, J. L. Rousset, and M. Broyer, Eur. Phys. J. D **16**, 201 (2001).
[30] J. Lermé, Eur. Phys. J. D **10**, 265 (2000).
[31] M. Brack, Rev. Mod. Phys. **65**, 677 (1993).
[32] V. V. Kresin, Phys. Rep. **220**, 1 (1992).
[33] A. Liebsch, Phys. Rev. B **48**, 11 317 (1993).
[34] J. Lermé, B. Palpant, B. Prével, E. Cottancin, M. Pellarin, M. Treilleux, A. Pérez, J. L. Vialle, and M. Broyer, Eur. Phys. J. D **4**, 95 (1998).
[35] V. V. Kresin, Phys. Rev. B **51**, 1844 (1995).
[36] L. Serra and A. Rubio, Z. Phys. D: At., Mol. Clusters **40**, 262 (1997).
[37] H. Ehrenreich and H. R. Philipp, Phys. Rev. **128**, 1622 (1962).
[38] C. Kittel, *Introduction to Solid State Physics* (Wiley, New York, 1983).
[39] The studied sizes $N=440$ up to 5670 are magic. This allows an easier and faster convergence for the iterative solving of the self-consistent ground-state Kohn-Sham equations, which is required in the TDLDA formalism.
[40] U. Fano, Phys. Rev. **124**, 1866 (1961).
[41] G. Mie, Ann. Phys. (Leipzig) **25**, 377 (1908).
[42] H. Hövel, S. Fritz, A. Hilger, U. Kreibig, and M. Vollmer, Phys. Rev. B **48**, 18 178 (1993).